Investigation of Quench Sensitivity and Microstructure Evolution During Isothermal Treatment in 2195 Al–Li Alloy

Zhiwu Zhang[1,2] · Youping Yi[1,2,3] · Wen You[4] · Shiquan Huang[2,3] · Yonglin Guo[4] · Hailin He[1,2]

Abstract

To investigate the quenching sensitivity of the 2195 Al–Li alloy rolled sheet and guide the design of the quenching process, the time–temperature-property (TTP) curves of this material were researched through interrupted quenching experiments. The differential scanning calorimetry (DSC) and transmission electron microscope (TEM) were used to characterize the evolution of precipitates during isothermal treatment. The results of this essay demonstrated that the nose temperature of 2195 Al–Li alloy is around 370 °C and the temperature range of quenching sensitivity is 340 °C to 400 °C. The microstructure observation revealed that the T_1 particles precipitate and grow rapidly at the temperature from 340 to 400 °C, which is due to the high nucleation rate of phase and fast solute diffusion kinetics, especially at the nose temperature. The needle-shaped θ'/θ'' and T_1 particles grow up quickly as the isothermal preservation time prolonged, leading to the decrease of the supersaturated solid solution of the matrix. This will reduce the number of the age-induced precipitate and weaken the subsequent age hardening effect. Therefore, the rate of cooling should be increased in the quenching sensitivity range (340–400 °C) to inhibit the precipitation of the second phase and obtain excellent mechanical properties. While in other temperature ranges, the cooling rate should be decreased appropriately to reduce residual stress. The appropriate average cooling rate is recommended to be around 13 °C s^{-1} at the temperature from 340 to 400 °C.

Keywords 2195 Al–Li alloy · Quenching sensitivity · Phase formation · TTP curve · Microstructure

1 Introduction

Recently, Al–Li alloys have been extensively applied in aerospace, commercial applications, and military which strongly require stiffness-critical and weight-critical structures [1–3]. Due to the beneficial combinations of high specific strength and stiffness, low density, high elastic modulus, excellent corrosion resistance, and welding, 2195 Al–Li alloy is being considered for cryogenic tank applications on the next launch vehicles [4–7]. Three procedures of quenching, solution treatment, and artificial ageing are generally used to obtain excellent mechanical properties of aluminum alloy [8]. It's worth noting that the 2195 Al–Li alloy, as a kind of aluminum alloy with high quenching sensitivity, need to keep a fast enough quenching cooling rate. Otherwise, the supersaturated solid solution will quickly decompose and cannot form a high degree of supersaturated solid solution; then its performance will be corresponding significantly reduced compared with the peak value during the subsequent ageing process [9, 10]. However, the excessive rapid cooling rate will cause excess residual stress in the material, which will cause the workpiece to distort during the subsequent processing [11]. Therefore, the residual stress and the mechanical performance should be appropriately matched by selecting a reasonable cooling rate [12–14], and the quenching sensitivity of this alloy is of great significance to its quenching process in industrial production [15].

✉ Youping Yi
yyp@csu.edu.cn

✉ Shiquan Huang
huangshiquan@csu.edu.cn

1 Light Alloy Research Institute, Central South University, Changsha 410083, China

2 State Key Laboratory of High Performance Complex Manufacturing, Central South University, Changsha 410083, China

3 School of Mechanical and Electrical Engineering, Central South University, Changsha 410083, China

4 Southwest Aluminum Group Co., Ltd, Chongqing 401326, China

Nowadays, the temperature–time-property (TTP) curve, as an effective way to study the quench sensitivity, can comprehensively reflect the isothermal transformation process of materials under different degrees of undercooling [16–18]. TTP curve combined with a quenching factor method can predict its hardness, strength, and fracture properties [19–21]. Li et al. [22] disclosed that the quenching sensitive temperature of 6063 aluminum alloy is 280–410 °C by using these diagrams. B.Milkereit and M.J.Starink [10] introduced a physically-based model that is used to model the precipitation in the matrix during the quenching process and simulate the strength after cooling and after subsequent age hardening. Meanwhile, there has been considerably researched on the quenching sensitivity of the Al–Zn–Mg–Cu alloys [23, 24]. Nevertheless, there is little information about the TTP curves of Al–Cu–Li alloys to guide the production.

This study aims to reveal the quenching sensitivity of the 2195 Al–Li alloy by the interrupted quenching technique. The hardness test of the material was carried out to study the evolvement of the mechanical properties during the whole quenching process. According to the above data, the TTP curves were determined and the quenching sensitivity of this alloy was analyzed to control and improve the quenching method of 2195 Al–Li alloy. Furthermore, 2195 Al–Li alloy, as a representative third-generation Al–Li alloy, has a more complicated chemical composition and the second phase precipitation behavior than other aluminum lithium alloys [25]. The effect of the adding chemical element composition on the microstructure and mechanical performance of this material has been researched in latest literature. Rioja et al. [26] concluded that the influences of some adding elements on the texture, microstructure, and mechanical performance of 2195 Al–Li alloy, such as adding Zr and Mn elements for regulating recrystallization and texture, adding Zn elements for corrosion improvement and solid-solution strengthening, adding Ag and Cu elements for precipitation strengthening and solid-solution, and adding Li and Mg for precipitation strengthening, density reduction, and solid-solution. In addition, to clarify the precipitation mechanism of the phases of the experimental alloy in the quenching sensitivity range, the microstructural characteristic during the isothermal treatment was also studied. The results in this research can provide critical process parameter for the quenching process of 2195 Al–Li alloy rolled sheet.

2 Materials and Experimental Methods

The experimental alloy was cut from a thick 2195 Al–Li alloy rolled sheet ($2800 \times 1500 \times 12$ mm), and the Table 1 is the chemical element composition. Specimens with dimensions of $15 \times 15 \times 5$ mm were prepared to measure the hardness. The specimens were transferred to the salt bath quickly (< 3 s) after isothermal holding in an air furnace at 510 °C for 1 h, and kept isothermally at a temperature of 250 °C to 470 °C for a set time, and then immediately quenched into cold water, finally performed T8 artificial ageing (3% pre-deformation $+ 160$ °C $+ 24$ h).

The hardness was gauged using Vickers indenter and the applied load was 1 kg for 30 s after T8 artificial ageing. Each sample was tested at least five times while the average value was used. In a purified argon atmosphere, the DSC analysis was carried out using DSC 8500 to analyze the thermal behavior of the samples and evaluate the microstructural evolution. The height and the diameter of specimens were 4 mm and 3 mm, respectively. The specimens heated at a rate of 10 °C min^{-1} from 50 to 470 °C. The samples for transmission electron microscope (TEM) test were achieved by mechanical grinding and electropolished using a Struers TenuPol electropolisher in an electrolytic solution containing 70% methanol and 30% nitric acid below -28 °C. The microstructures of the experimental material were undertaken in a Titan G^2 60–300 TEM operating at 300 kV.

3 Results

3.1 The Influence of Different Isothermal Temperature and Time on Hardness

The hardness of as-aged specimens processed by different isothermal treatment is illustrated by Fig. 1. According to the former research results [27, 28], the trend of the hardness curve is consistent with the phase transition. Figure 1 shows that the hardness value of samples, in the process of different isothermal holding temperature, generally decreases with the prolongation of holding time. However, the development of the hardness is closely related to the isothermal preservation time and temperature. For example, when the holding time is less than 600 s, the hardness decreases quickly, and after continuing to extend to 1200 s, the rate of decrease tends to be stable. It is to be noted that the hardness value of 2195 Al–Li alloy keeps stable after being held for 1200 s in the temperature range of 340–470 °C, but when kept at 250–310 °C, that is still

Table 1 Chemical element composition of the experimental alloy (wt%)

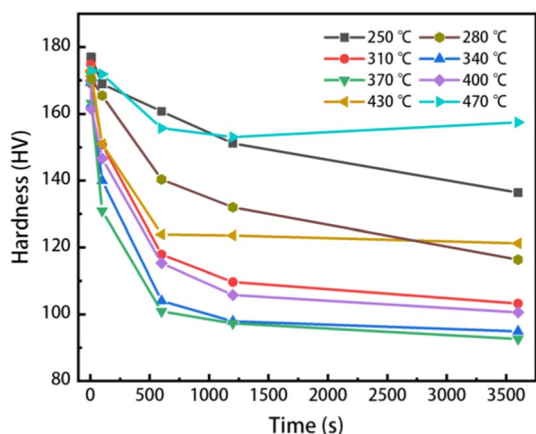| Alloy	Li	Cu	Mg	Zr	Mn	Ag	Fe	Si	Al	Other
2195	0.9	4.1	0.28	0.13	0.28	0.26	0.04	0.03	Bal	< 0.1

Fig. 1 Vickers hardness variation of as-aged specimens after isothermal heat preservation at various temperatures for diverse time: 250–470 °C

decreasing until the isothermal time exceeds 3600 s. Particularly, after incubation at 370 °C for various time, the property of the 2195 Al–Li alloy decreases rapidly. And when the specimen is kept at 370 °C for 600 s, the hardness drops from 163 to 101 HV, reducing by 38%. After extending the holding time to 1200 s, the hardness decreases to 98 HV, reducing by 42% and the rate of decline is significantly reduced within 3600 s. However, when the temperature remained at 250 °C for 600 s, the hardness value drops from 177 to 161 HV, which is only a decrease of 9%. After being kept for 3600 s, the hardness value reduces to 136 HV, reducing by 23%. According to the hardness curve of the as-aged alloy, the hardness of the sample decreases rapidly, covering the temperature range 340–400 °C, and the hardness change is relatively small when the temperature is higher or lower than this temperature range.

3.2 TTP Curve

To further study the quenching sensitivity of 2195 Al–Li alloy rolled sheet, the quenching sensitivity temperature range should be determined. As an essential way to evaluate the quench sensitivity, TTP curve is used in this article. EVANCHO and STALEY [19] investigated the kinetics of aluminum alloy continuous cooling precipitation. They found that the critical time required for the precipitation of quantitative solute atoms from the matrix satisfies a particular relationship between the critical time and temperature, that is the TTP curve. Its expression is as follows:

$$C(T) = -k_1 * k_2 * \exp\left\{\frac{k_3 * k_4^2}{R * T * (k_4 - T)^2}\right\} * \exp\left(\frac{k_5}{R - T}\right) \tag{1}$$

where k_1 represents the natural logarithm of the untransformed fractions; k_2 represents a constant associated with the

reciprocal of the quantity of nucleation sites; k_3 represents a constant associated with the energy demanded to generate a nucleus; k_4 represents a constant associated with the solvus temperature; k_5 represents a constant associated with the activation energy for diffusion; T represents absolute temperature; R represents the gas constant.

In this research, the 95% peak hardness of the aged sample without isothermal treatment (the hardness value of the T8 ageing state after water quenching at room temperature is 178 HV) is used to fit the Eq. (1). The fitted TTP curve of the experimental alloy is shown in Fig. 2 and the parameter values in the equation after fitting are shown in Table 2.

According to the TTP curve fitting parameters and Eq. 1 obtained above, the fitting curves of 99.5%, 95%, and 90% of the maximum hardness of experimental alloy can be obtained, as shown in Fig. 2. There is serious quenching sensitivity when the temperature range is 340–470 °C, especially, the temperature is about 370℃, as illustrated in Fig. 2. C(T) function can effectively predict the incubation time of the test material. When the hardness decreases about 5% at 370 °C, the critical time is 4.5 s. However, it takes about 187 s for the performance to drop to 95% of the maximum value when the preservation temperature is far from the quenching sensitivity temperatures such as 470 °C. Therefore, it is necessary to strictly control its cooling rate in the sensitive range to obtain products with excellent performance. The critical average cooling rate is recommended to be around 13 °C s⁻¹ to obtain 95% of the maximum performance at the quenching sensitivity temperature.
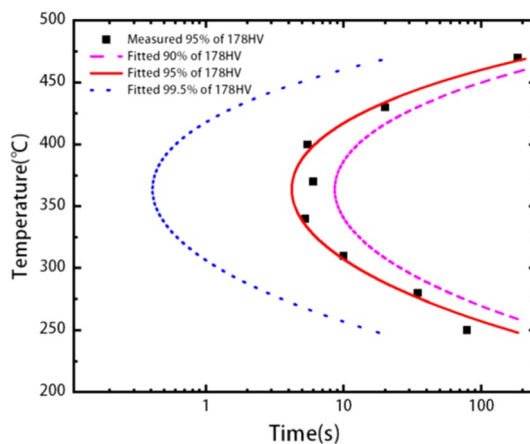

Fig. 2 TTP curve for 2195 aluminum–lithium alloys

Table 2 Coefficient of fitting TTP curve equation of 2195 Al–Li alloy

K_2/s	K_3/(J mol⁻¹)	K_4/K	K_5/(J mol⁻¹)
3.7×10^{-9}	8443	716	37,152

3.3 DSC Experiment

In order to research the precipitation kinetics of the experimental alloy, it has been conducted on the aged samples held various time at 250 °C and 340 °C by the DSC technique, as shown in Fig. 3. The Al–Cu–Li alloys have a complicated precipitation mechanism. Jo and Hirano [29] found that the predominant strengthening phases of Al–Li alloy are δ′ (Al$_3$Li), T$_1$ (Al$_2$CuLi), and θ″/θ′ (Al$_2$Cu). The phases which precipitate from the supersaturated solution depends on Cu/Li concentration (wt%) ratios and the precipitation sequences have been suggested to be as follows: supersaturated solution → G.P.zones → (δ′ + G.P.zones) → (δ′ + θ″) → (δ′ + θ′) → (δ′ + T$_1$) → T$_1$. The T$_1$ equilibrium phase is semi-coherent with the aluminum matrix by a hexagonal close-packed structure. The δ′ metastable phase is completely coherent with the aluminum matrix by a face-centered cubic structure, and the θ″/θ′ metastable phase is coherent/semi-coherent with the aluminum matrix by a cubic structure [25]. According to the DSC thermograms [30, 31], the exothermic peak is related to the precipitation of the second phase, and the endothermic peak represents the dissolution of the former second phase. The area below the amplitude or the peak represents the number of the dissolution or precipitation of the second phase [32, 33].

From the DSC results, several endothermic and exothermic events were confirmed. The endothermic peak which is marked as A can be found due to the dissolution of G.P. zones and clusters that are already formed in the specimen at room temperature [16, 34]. When the holding time is extended to 1200 s, this endothermic peak gets smaller and smaller (Fig. 3a) until it finally disappears (Fig. 3b). Owing to the dissolution of δ′ phase, a tiny peak attaching to the major peak C on the curve (marked by B) is observed, and it can be found to be around 208 °C [30].

On the one hand, due to 2195 Al–Li alloy belongs to the third generation of aluminum–lithium alloys, and they all contain less than 2 wt% of Li, which greatly inhibits the formation of δ′ phase [35]. On the other hand, when the sample is kept for a long time in the quenching sensitivity temperature, a large amount of coarse second phase has been precipitated from the matrix, and the subsequent precipitation power is greatly reduced, and thus, the B peak disappears finally [36]. And peak C is a large exothermic peak, which means the T$_1$ phases are formed [34]. When held at 250 °C for different time, the peak gradually decreases as the isothermal preservation time prolonged, which is consistent with the reasons stated earlier. Moreover, according to Fig. 3b, when the preservation temperature is in the quenching sensitivity (340 °C), the peak C finally disappears as the holding time extended to 1200 s. Dorin et al. [36] researched the evolution during continuous heating of 2198 alloy ageing 18 h at 155 °C (similar to a T8 state) through DSC and SAXS (small-angle X-ray scattering), and they disclosed that owing to the thickening of T$_1$ phases, a secondary exothermic peak is formed between 300 °C and 350 °C. This phenomenon corresponds to peak D. According to the research of Q. Chu et al.[34], the endothermic peak E corresponds to the dissolution of the T$_1$ phase.

With the prolongation of the isothermal preservation time, the peak value is smaller than before (Fig. 3b). When the preservation time extends to 1200 s and the holding temperature is 340 °C, only one exothermic peak marked by D is observed, which is consistent with the fact that most of the solute atoms in the matrix have been completely eluted and precipitated with the extension of the holding time[37]. From the previous discussion, we can know that the T$_1$ phase is the dominating precipitate in the matrix, and the equilibrium phase T$_1$ can be recognized as
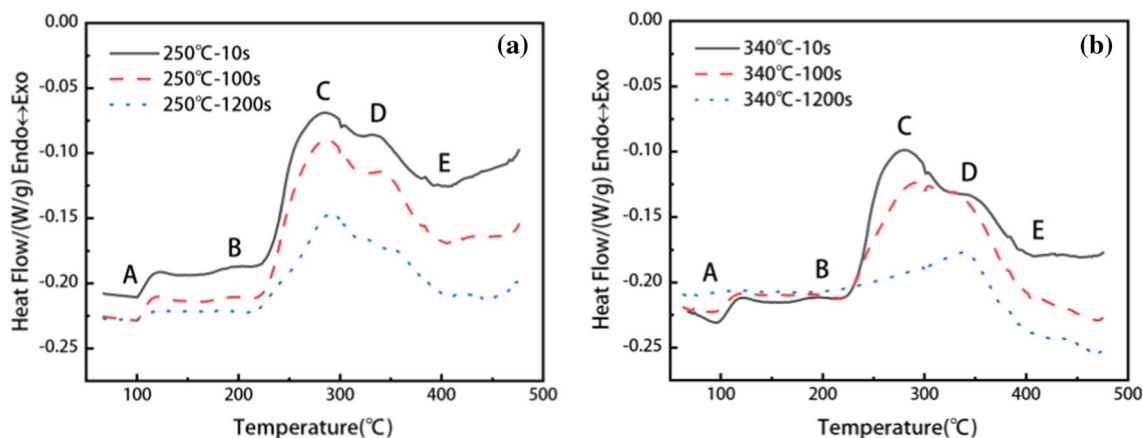

Fig. 3 DSC thermograms of 2195 aluminum–lithium alloy obtained at different isothermal preservation time at **a** 250 °C; **b** 340 °C with a heating rate of 10 °C min^{-1}

the predominant strengthening precipitate in the ageing process with the prolongation of isothermal preservation time.

3.4 TEM Microstructure Observation

To further clarify the precipitation mechanism of the precipitated phase of the 2195 Al–Li alloy in the quenching sensitivity range, according to the above TTP curve and DSC curve, this part researched the precipitation behavior of the precipitate of the material in the quenching sensitivity temperature. As a traditional third-generation Al–Li alloy, the 2195 Al–Li alloy has complex precipitates, such as θ′/θ″ phase, T_1 phase, and S phase [2]. P. Donnadieu et al. [38] studied the construction of T_1 phases which presented under ageing in Al–Li–Cu alloys. They concluded that the interface with the aluminum matrix generates on the Al–Cu mixed layer of the T_1 phase and the thickness of T_1 precipitate is smaller than one cell.

Figure 4 illustrates the microstructure of as-aged specimens with different isothermal treatment, which was taken along the < 110 >$_{Al}$ direction. Selected area diffraction (SAD) pattern corresponding to TEM taken along [110] zone axis can show the presence of T_1 phase [36, 39]. From Fig. 4a–c, the microstructure of the specimen is influenced by the isothermal holding time. A great

number of dislocations are observed when the sample does not hold isothermally, as shown in Fig. 4a. Meanwhile, a certain amount of needle-shaped second phase is found in the matrix. The density of the small precipitate is plainly reduced and the uneven second phases are distributed in the matrix (Fig. 4b), as the isothermal preservation time prolonged to 10 min. Compared with the standard diffraction pattern along < 110 > zone axis (Fig. 4e) and other research [40–44], it can be verified that the needle-like second phase is T_1 phase, which has a hexagonal platelet structure (lattice constants c = 0.935 nm and a = 0.496 nm). The crystallographic orientation relationships between the matrix and T_1 phase are [110]$_{Al}$ // [1010]$_{T1}$ and [111]$_{Al}$ // [0001]$_{T1}$. When the holding time reaching 20 min, the T_1 phase increases by 16 times (2 μm) compared with the sample without heat preservation (120 nm), as shown in Fig. 6c. According to Fig. 4, the dislocation and the solute atoms in the matrix are consumed as the isothermal holding time prolonged, which greatly undermines the subsequent age hardening effect. With the growth and coarsening of the second phase, the dislocation in the matrix is significantly consumed. Simultaneously, the line appearing with the red circle in the SAD pattern becomes blurred, which represents the existence of T_1 phase. So with the prolongation of the isothermal preservation time, the T_1 phases gradually grow up and become the main phase in the matrix, and the number of T_1 precipitates
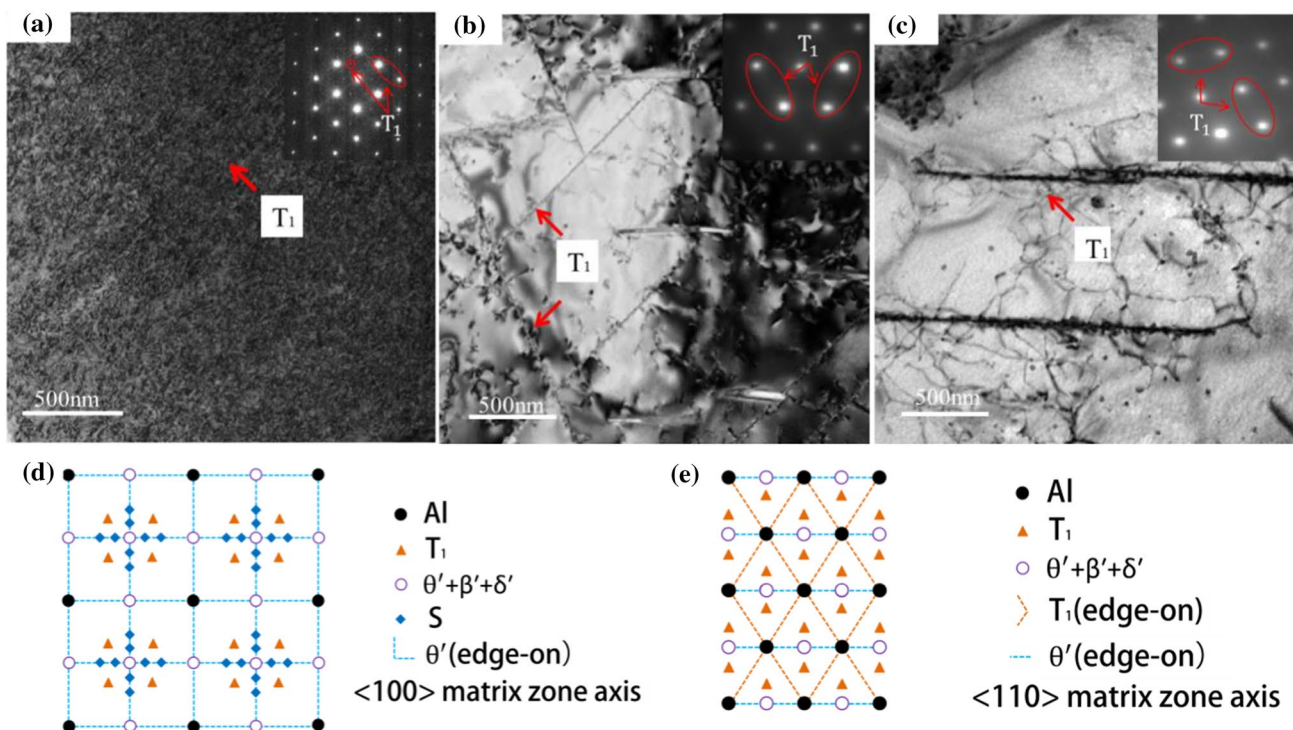

Fig. 4 TEM bright field photographs of the as-aged 2195 Al–Li alloy after isothermal preservation for various time at 370 °C and the corresponding SAD pattern at the upper right corner: **a** 0 min, **b** 10 min, **c** 20 min, **d** standard diffraction pattern along < 100 > zone axis, **c** standard diffraction pattern along < 110 > zone axis

decreases rapidly, which can also be confirmed by the SAD pattern in Fig. 4. Note that this is consistent with DSC analysis.

Figure 5 shows the high-angle annular dark filed-scanning transmission electron microscope (HAADF-STEM) photographs of the 2195 Al–Li alloys after holding at 370 °C temperature for different holding time. Figure 5a–c were taken along the $< 110 >_{Al}$ direction, and Fig. 5d–f were taken along $< 100 >_{Al}$ direction. θ′/θ″ phases are formed on the {100} matrix planes and T_1 phases are formed on the {110} matrix planes. There are crystallographic orientations at the bottom right of each photo [45]. The θ′ phase, as a semi-coherent, metastable precipitate, has a stable tetragonal crystal structure (lattice parameters a = 0.404 nm and c = 0.580 nm) [46]. When researched the TEM diffraction patterns, the orientation and shape of the θ′ precipitate cause the development of streaks along the $< 110 >_{Al}$ directions [47]. It is first proposed that the S phase is an orthogonal crystal according to the XRD study of Westgren and Perlitz [44]. And the lattice parameters are tested subsequently by Mondolfo (lattice constants a = 0.4 nm, b = 0.925 nm, and c = 0.718 nm). Along the $< 100 >_{Al}$ direction, the S phases form primarily as wattles on the {210} habit planes [48].

The sample without heat preservation treatment, after T8 heat treatment, has lots of uniform and fine second particles in the matrix, according to the Fig. 5a. The T_1 phases precipitated on the {110} matrix planes are homogeneously distributed in the crystal and grain boundary. Meanwhile, there are some needle-shaped phases that are perpendicular to each other and long strip phases (Fig. 5d). According to Fig. 4e, it is certain that these phases are a composite of θ′/θ″ phases and S phases [42, 49, 50]. The θ′/θ″ phases precipitated along the {100} matrix planes are dispersed and distributed in the crystal, while the quantity of θ′/θ″ phases is small and the length is between 40–100 nm. However, the number of θ′/θ″ phases has been significantly reduced as the holding time prolonged, but the size is basically not changed (Fig. 5b). Similarly, a small amount of S phase is found, but it decreases rapidly as the holding time extending and the diffraction line in the upper right corner diagram eventually disappears. After being kept for 10 min, according to Fig. 5c, the T_1 phases have grown rapidly and the length exceeds
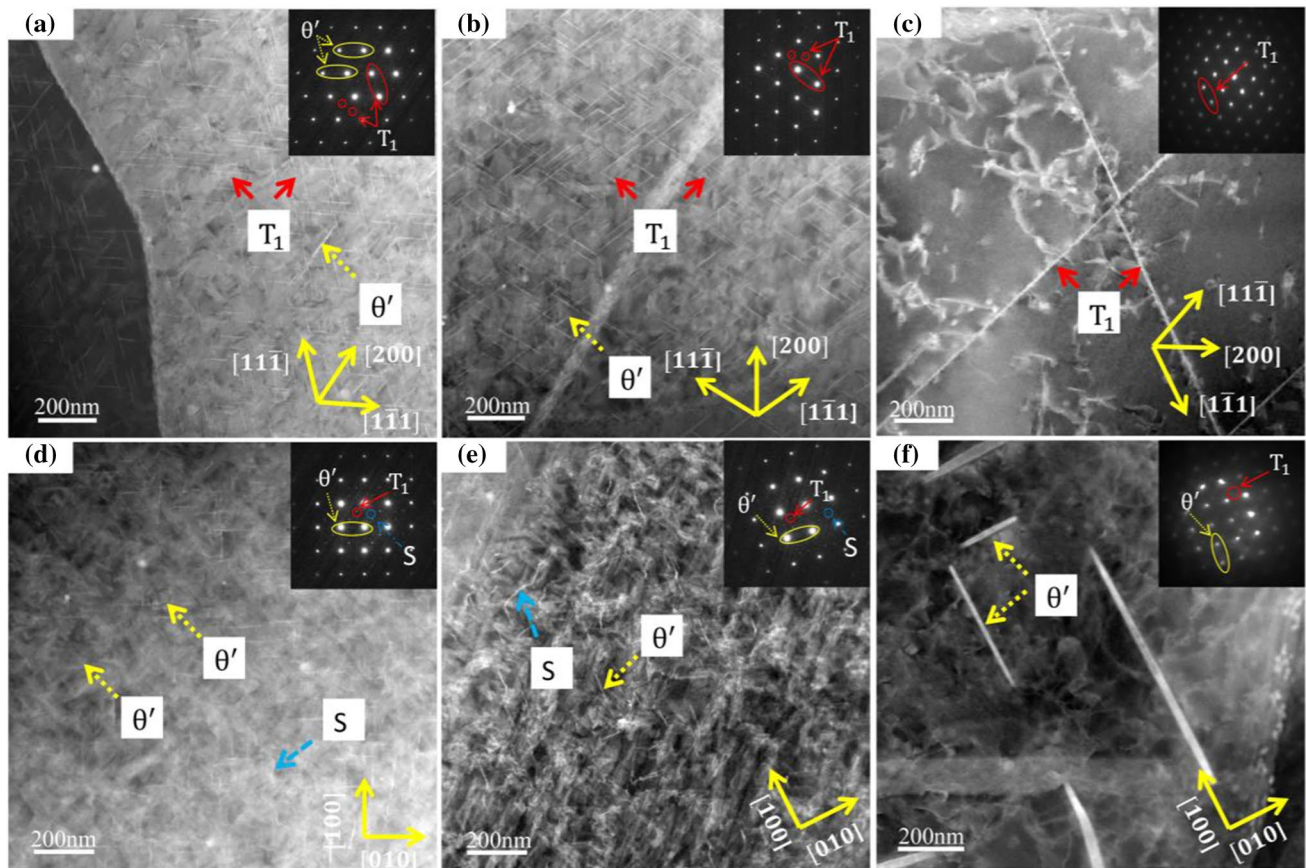

Fig. 5 HAADF-STEM photographs of the as-aged specimens after isothermal preservation for various time at 370 °C and the corresponding SAD pattern at the upper right corner; **a**, **d** 0 s; **b**, **e** 100 s; **c**, **f** 600 s. **a–c** were taken along $< 110 >_{Al}$ matrix zone axis, and **d–f** were taken along $< 100 >_{Al}$ matrix zone axis

1.5 μm, with its number reducing considerably. Simultaneously, the number of θ′/θ″ phases also greatly reduces, and its size increases. It could be clearly seen that the S phases are greatly reduced as the holding time increases (Fig. 5d–f). These can also be proved by the change of the line with the yellow and blue circle in the SAD pattern and even the line with the blue circle disappears eventually (Fig. 5f). The lines in the SAD pattern become inconspicuous.

As shown in Fig. 6, the precipitate length distribution (PLD) based on the above is analyzed. To ensure the credibility of these statistics, at least three STEM pictures are measured and the number of second phases measured is more than 200. The whole process is performed through the software: Image Pro Plus. The length of the T_1 phases is basically between 60–120 nm and the PLD is concentrated in an average of 89 nm as the sample without heat preservation treatment (Fig. 6a). According to Fig. 6b, the T_1 phases grow slightly when the samples are kept for 10 s, and the length is basically between 100–180 nm. According to the literature [45], T_1 phases and θ′/θ″ phases have

a competitive precipitation relationship during the ageing process. The precipitation and rapid growth of T_1 phases consume the θ′/θ″ phases in the matrix and limit the θ″ transfer to θ′. As vividly revealed by Fig. 6a–c, the T_1 phases gradually grow up when the isothermal holding temperature prolonged. Therefore, the uniform and fine θ′/θ″ phases in the matrix are greatly reduced. Similarly, the uniform and fine θ′/θ″ phases have basically disappeared and only some thick θ′/θ″ phases exist, as shown in Fig. 5d–f. Because of long heat preservation, the matrix lost a lot of solute atoms, which greatly inhibits the precipitation of the fine and uniform second phases during the later ageing [51]. Therefore, the properties of the alloy are adversely affected.

Figure 7 shows many needle-shaped second phases which precipitate along the grain boundaries under various isothermal preservation time at 370 °C. As for the specimen without isothermal holding treatment, the fine second precipitations are distributed along the grain boundary (Fig. 7a). As the isothermal preservation time prolonged to 10 s, according to Fig. 7b, the grain boundary is increased from 32 to
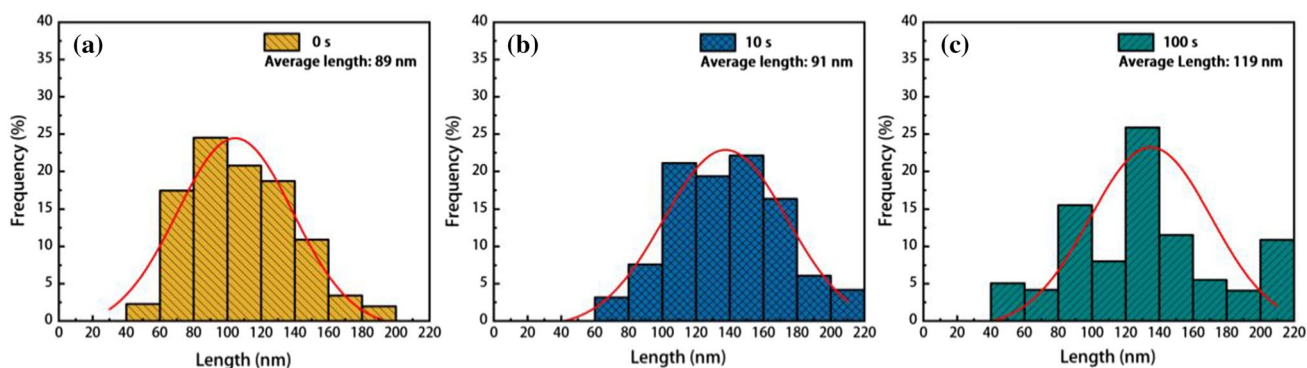

Fig. 6 The precipitate length distribution of T_1 phases in 2195 Al–Li alloy with various isothermal holding time at 370 °C: **a** 0 s; **b** 10 s; **c** 100 s
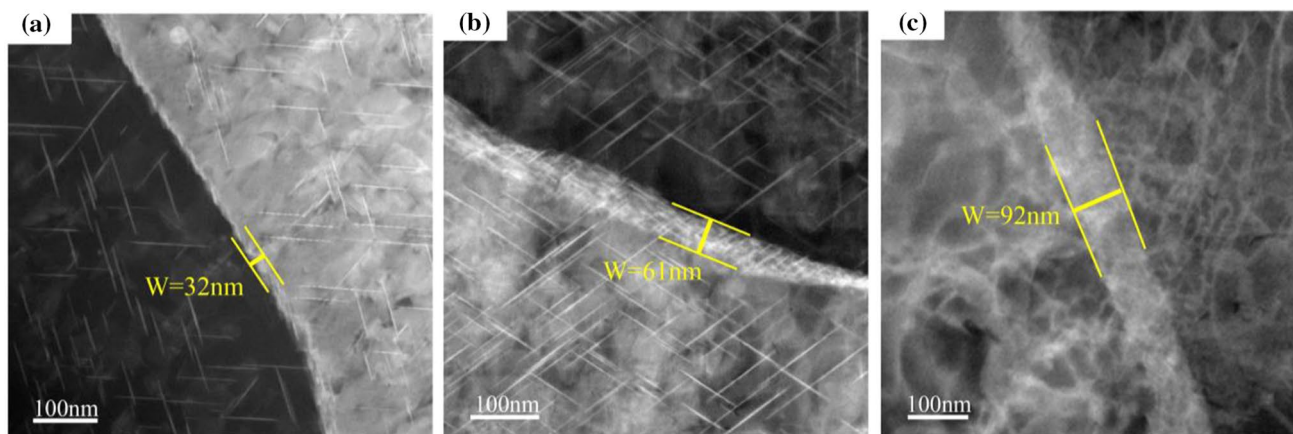

Fig. 7 $<110>_{Al}$ STEM micrographs of the as-aged 2195 Al–Li alloy after isothermal preservation for various time at 370 °C: **a** 0 s; **b** 10 s; **c** 10 min (W = 32 nm refers to the width of the grain boundary is 32 nm)

61 nm. It shows more and finer second phase at the grain boundary and the number of the second phases around the grain boundary is small. This is because the grain boundary has higher energy than the inside grain and the second phase preferentially precipitates here. In the meantime, the content of solute atoms around the grain boundary also decreases greatly, which leads to the emergence of an obvious precipitate free zone (PFZ). As the sample kept for 10 min, the precipitated phase on the grain boundary basically disappeared, and the grain boundary increased to about 92 nm (Fig. 7c). Noted worthy to mention is that most of the second phases have disappeared, no matter the grain or the grain boundary. This is due to a large number of solute atoms are consumed by the coarse precipitation of the grain boundary during the isothermal holding process. This is consistent with the situation explained by DSC. When the alloy is kept in the quenching sensitive area, abundant coarse second phases will precipitate in the matrix, which greatly reduces the supersaturation of the matrix. During the ageing treatment, the precipitation power is greatly reduced, and the fine and uniform second phase cannot be precipitated, which seriously reduces the performance of the alloy.

4 Discussion

According to the analysis in the previous section, as the prolongation of isothermal preservation time during quenching, the precipitation phase of the experimental alloy will grow up and coarsen, affecting the strengthening effect of the second phase in the later ageing period. The TTP curve of 2195 Al–Li alloy is "C" shape, according to Fig. 2, and its quenching sensitivity range is between 340–400 °C. The second phase has the fastest precipitation rate at 370 °C. On both sides of the nose temperature, the second phase precipitation rate decreases. The second phase precipitation rate is small as the isothermal holding temperature kept away from the nose temperature. However, the reasons for the decrease of precipitation rate in low temperature regions and high temperature regions are different. During the quenching time, the quenching sensitivity of this alloy is linked with the alloy composition and nucleation position [52]. And the nucleation rate I can be expressed by:

$$I = c * \exp\left(-\frac{\Delta G^* + Q}{k * T}\right) \tag{2}$$

where Q represents the solute diffusion activation energy, c represents a constant, ΔG^* represents the nucleation activation energy, T represents the absolute temperature, and R represents the gas constant. From Eq. (2), the isothermal holding temperature has a great effect on the precipitation rate and growth of the second phase. In the low temperature

range, the solid solution of the material has a large degree of supersaturated and the precipitation power is sufficient. However, due to the low temperature and the low atomic diffusion rate, the nucleation rate of the second phase is very small. On the contrary, although the material has a high atomic diffusion rate in the high temperature range, the supersaturated of the alloy solid solution decreases, and the nucleation rate is inhibited due to insufficient precipitation power. Consequently, the precipitation rate of the second phase is not high. In the medium temperature region, the atomic diffusivity and material supersaturated are large, and the second phase can precipitate and grow up quickly. Therefore, a large amount of second phase precipitation occurs in the quenching sensitive area. So it has the highest quenching sensitivity in the middle temperature range. This is basically consistent with the results obtained by the previous DSC and TEM observations.

Aluminum alloy can be strengthened by uniform and fine second phases. The smaller the precipitated second phase, the better the strengthening effect. For the aluminum–lithium alloy studied in this study, according to Figs. 4 and 5, the second phase grows up quickly and the density of dislocations in the matrix is greatly reduced with the prolongation of holding time. Especially in the quenching sensitive range, the precipitation rate is greatly accelerated and the coarse second phase is precipitated, resulting in a large loss of solute atoms. In the subsequent ageing process, a fine and uniform second phase cannot be precipitated, leaving only some coarse second phases in the matrix, which seriously damages the properties of the material. Based on the above investigation, the diagrams of second phase precipitation for the as-aged sample after holding at 370 °C as the holding time prolonged are schematically illustrated in Fig. 8. In the early period of isothermal preservation at the nose temperature, only a small amount of T_1 and θ' phases are formed, and the fine second phase precipitates during the subsequent ageing process. The T_1 and θ' phases will precipitate and grow up quickly and different second phases compete for solute atoms as the prolongation of isothermal holding time. This will reduce the supersaturation of the matrix, which will make the fine second phase cannot be precipitated. So there are only some coarse second phases in the matrix after ageing (Figs. 4c, 5c). Therefore, when plastic deformation is carried out, the dislocation can easily bypass these coarse second phases, and the pinning effect of the second phase is greatly weakened, which makes the properties of the alloy decrease obviously. When the heat preservation temperature is close to the nose temperature, the hardness has a sharp decline as the isothermal preservation time extended. This explains why the hardness reduction rate is different at different temperatures in Fig. 1.

The TTP curve of 2195 Al–Li alloy studied in this article (Fig. 2) shows that the incubation period of quenching is

Fig. 8 Precipitation scenario for the as-aged experimental alloy after isothermal holding at 370 °C as the holding time prolonged
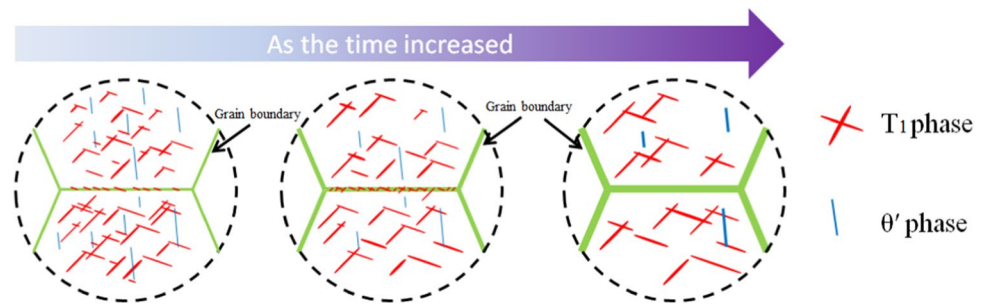
very short in the narrow temperature range around 370 °C, and it is only 4.5 s. It reflects the quenching sensitivity of the alloy: the quenching sensitivity is serious when the incubation period is transitory. As the incubation period prolonged, the supersaturated solid solution is stable, which means the low quenching sensitivity. The incubation period can be long when the quenching temperature is far from the nose temperature. For example, the incubation period is 187 s when the isothermal preservation temperature is 470 °C. Therefore, the cooling rate of the alloy should be increased at the quenching sensitivity. In the actual production process, the supersaturated solid solution decomposes hardly as the rate of cooling increased, and it will precipitate the dispersed phase with uniform distribution in the subsequent ageing process, so the best age hardening effect will be achieved. However, due to the influence of thermal stress, too fast cooling rate will cause excessive residual stress on material, which leads to the serious deformation of the subsequent sample, so the properties of the parts can be worse. In order to prevent the precipitation of solute atoms in quenching sensitive zone, the cooling rate should be increased in the 340–400 °C to inhibit the precipitation of the second phase, while in other temperature sections, the cooling rate should be reduced appropriately to balance residual stress and thus obtain higher comprehensive properties. In the quenching sensitive temperature range, a cooling rate of 16 °C s^{-1} is recommended to obtain 95% of the maximum performance.

5 Conclusion

In this research, the quenching sensitivity of the 2195 Al–Li alloy was investigated by the TTP curve, DSC, TEM, and STEM methods, which were applied to analyze the microstructural evolution. According to the analysis of the results, the conclusions are summarized as following:

1. The TTP curve has been obtained for 2195 Al–Li alloy, and the quenching sensitivity ranges and the critical coefficients are identified. The temperature range of quenching sensitivity is between 340 °C to 400 °C, and the critical temperature is 370 °C.

2. Owing to the uneven precipitation of coarse T$_1$ phases, the 2195 Al–Li alloy has high quench sensitivity, which will seriously affect the properties of the alloy.

3. According to the analysis of TEM and DSC curves, the decomposition rate of supersaturated solid solution is very fast when the nose temperature is 370 °C. Simultaneously, the sparse θ′ phases and abundant T$_1$ phases will be precipitated and coarsened in the matrix. The supersaturated solid solubility of the matrix is greatly reduced, which inhibits the precipitation of other phases and further weakens the effect of subsequent age hardening.

4. To balance mechanical performances and the residual stress of this material, it is recommended to increase the rate of cooling in the quenching sensitivity temperature range, and suppress the cooling rate in other temperature ranges. It is suggested to cool at a cooling rate of 16 °C s^{-1} to obtain 95% of the maximum performance in the quenching sensitive temperature range.

References

1. S.Y. Betsofen, V.V. Antipov, M.I. Knyazev, Russ. Metall. **2016**, 326 (2016)
2. S. Nouri, S. Sahmani, M. Hadavi, S. Mirdamadi, Met. Mater. Int. **26**, 1134 (2020)
3. M. Ubaid, D. Bajaj, A.K. Mukhopadhyay, A.N. Siddiquee, Met. Mater. Int. **26**, 1841 (2020)
4. S.V.S.N. Murty, A. Sarkar, P.R. Narayanan, P.V. Venkitakrishnan, J. Mukhopadhyay, Mater. Sci. Eng. A **677**, 41 (2016)
5. R.J. Rioja, Mater. Sci. Eng. A **257**, 100 (1998)
6. T. Dursun, C. Soutis, Mater. Design **56**, 862 (2014)
7. G. Kakauridze, B. Kilosanidze, in *Proceedings of SPIE*, ed. by H.I. Bjelkhagen. SPIE OPTO 2011, San Francisco, 23, 24, 26 January 2011. Vol. 7957, Practical Holography XXV: Materials and Applications (SPIE, Washington, 2011), p. 79570T
8. H. Wang, Y. Yi, S. Huang, J. Alloy. Compd. **690**, 446 (2017)
9. A. Deschamps, Y. Bréchet, Scripta Mater. **39**, 1517 (1998)

10. B. Milkereit, M.J. Starink, Mater. Design **76**, 117 (2015)
11. J.S. Robinson, R.L. Cudd, D.A. Tanner, G.P. Dolan, J. Mater. Process. Tech. **119**, 261 (2001)
12. B. Yang, B. Milkereit, Y. Zhang, P.A. Rometsch, O. Kessler, C. Schick, Mater. Charact. **120**, 30 (2016)
13. B. Milkereit, N. Wanderka, C. Schick, O. Kessler, Mater. Sci. Eng. A **550**, 87 (2012)
14. Y. Zhang, B. Milkereit, O. Kessler, C. Schick, P.A. Rometsch, J. Alloy. Compd. **584**, 581 (2014)
15. D.A. Tanner, J.S. Robinson, Mater. Design **29**, 1489 (2008)
16. E.Y. Kaputkin, Mater. Sci. Eng. A **280**, 76 (2000)
17. P. Archambault, D. Godard, Scripta Mater. **42**, 675 (2000)
18. X. Dai, C. Xiong, N. Li, Y. Luo, Rare Metal Mat. Eng. **48**, 721 (2019)
19. J.W. Evancho, J.T. Staley, Metall. Mater. Trans. B **5**, 43 (1974)
20. J.T. Staley, Mater. Sci. Tech.-Lond. **3**, 923 (1987)
21. M. Tiryakioĝlu, R.T. Shuey, Mater. Sci. Eng. A **527**, 5033 (2010)
22. H. Li, M. Han, C. Zeng,, Mater. Sci. Technol. **22**, 6 (2014)
23. M.J. Starink, B. Milkereit, Y. Zhang, P.A. Rometsch, Mater. Design **88**, 958 (2015)
24. B. Nie, P. Liu, T. Zhou, Mater. Sci. Eng. A **667**, 106 (2016)
25. C. Zhang, M. Liu, Z. Meng, Q. Zhang, G. Zhao, L. Chen, H. Zhang, J. Wang, J. Mater. Process. Tech. **283**, 116718 (2020)
26. R.J. Rioja, J. Liu, Metall. Mater. Trans. A **43**, 3325 (2012)
27. Y. Li, Z. Shi, J. Lin, Y.L. Yang, Q. Rong, B.M. Huang, T.F. Chung, C.S. Tsao, J.R. Yang, D.S. Balint, Int. J. Plasticity **89**, 130 (2017)
28. P. Ma, L. Zhan, C. Liu, Q. Wang, H. Li, D. Liu, Z. Hu, J. Alloy. Compd. **790**, 8 (2019)
29. H.H. Jo, K.-I. Hirano, Mater. Sci. Forum **13–14**, 377 (1987)
30. B. Cai, Z.Q. Zheng, D.Q. He, S.C. Li, H.P. Li, J. Alloy. Compd. **649**, 19 (2015)
31. B. Decreus, A. Deschamps, F. De Geuser, P. Donnadieu, C. Sigli, M. Weyland, Acta Mater. **61**, 2207 (2013)
32. A. Deschamps, M. Garcia, J. Chevy, B. Davo, F. De Geuser, Acta Mater. **122**, 32 (2017)
33. H. Sidhar, N.Y. Martinez, R.S. Mishra, J. Silvanus, Mater. Design **106**, 146 (2016)
34. Q. Chu, W.Y. Li, X.W. Yang, J.J. Shen, A. Vairis, W.Y. Feng, W.B. Wang, J. Mater. Sci. Technol. **34**, 1739 (2018)
35. H. Sidhar, R.S. Mishra, Mater. Design **110**, 60 (2016)
36. T. Dorin, A. Deschamps, F. De Geuser, W. Lefebvre, C. Sigli, Philos. Mag. **94**, 1012 (2014)
37. M.H. Tosten, A.K. VasudÉvan, P.R. Howell, Metall. Trans. A **19**, 51 (1988)
38. P. Donnadieu, Y. Shao, F. De Geuser, G.A. Botton, S. Lazar, M. Cheynet, M. De Boissieu, A. Deschamps, Acta Mater. **59**, 462 (2011)
39. O. Sitdikov, E. Avtokratova, M. Markushev, Met. Mater. Int. (2020). https://doi.org/10.1007/s12540-020-00842-2
40. W.B. Chen, D.H. Xiao, M.D. Wu, J. Huang, L.P. Huang, W.S. Liu, J. Mater. Res. Technol. **9**, 9675 (2020)
41. L. Wu, X. Li, H. Wang, Mater. Charact. **171**, 110800 (2021)
42. E. Balducci, L. Ceschini, S. Messieri, S. Wenner, R. Holmestad, Mater. Design **119**, 54 (2017)
43. T. Dorin, A. Deschamps, F. De Geuser, M. Weyland, in *ICAA13 Pittsburgh*, ed. by H. Weiland, A.D. Rollett, W.A. Cassada, 13th International Conference on Aluminum Alloys, Pittsburgh, 3-7 June 2012 (Springer, Cham, 2012), p. 1155
44. R.N. Lumley (ed.), *Fundamentals of Aluminium Metallurgy* (Woodhead Publishing, Cambridge, 2018)
45. H. Li, L. Zhan, M. Huang, X. Zhao, C. Zhou, and Z. Qiang, J. Alloy. Compd. **851**, 156829 (2021)
46. D. Shin, A. Shyam, S. Lee, Y. Yamamoto, J.A. Haynes, Acta Mater. **141**, 327 (2017)
47. J. Silcock, T. Heal, H. Hardy, J. I. Met. **82**, 239 (1954)
48. A.K. Gupta, P. Gaunt, M.C. Chaturvedi, Philos. Mag. A **55**, 375 (1987)
49. E. Balducci, L. Ceschini, S. Messieri, S. Wenner, R. Holmestad, Mater. Sci. Eng. A **707**, 221 (2017)
50. Q. Liu, R.H. Zhu, J.F. Li, Y.L. Chen, X.H. Zhang, L. Zhang, Z.Q. Zheng, T. Nonferr. Metal. Soc. **26**, 607 (2016)
51. N. Jiang, X. Gao, Z.Q. Zheng, T. Nonferr. Metal. Soc. **20**, 740 (2010)
52. B.C. Shang, Z.M. Yin, G. Wang, B. Liu, Z.Q. Huang, Mater. Design **32**, 3818 (2011)